TECHNOLOGIES FOR INSPECTION OF THE INDUSTRIAL AND GEOCHEMICAL ANOMALIES IN THE ATMOSPHERIC BOUNDARY LAYER

Yu.D. Kopytin, V.V. Nosov, and L.K. Chistyakova

Institute of Atmospheric Optics,
Siberian Branch of the Russian Academy of Sciences, Tomsk
Received January 21, 1997

We present new results obtained by the authors in the development of technologies for monitoring the atmospheric boundary layer (hereafter ABL) anomalies caused by the microgeochemical conditions or industrial pollution emissions.

INTRODUCTION

Original techniques and model setups designed for remote measurements of the aerosol composition and gas emissions from industrial plants have been developed in the laboratory of non-linear optical research at the Institute of Atmospheric Optics, Siberian Branch of Russian Academy of Sciences. These methods can be used in various investigations, e.g., for monitoring the microclimatic anomalies of both natural and anthropogenic origin. Instruments for remote detection of the pollution emissions (hereafter IDE) based on the passive correlation spectroscopy technique as well as the corresponding methods for remote atmospheric measurements and statistical filtration of the gas anomalies images observed on the background of underlying surface, are of certain interest because of their efficiency, simple design, and reliability. Coherent-optics method of the size distribution function retrieval based on the analysis of the speckle structure of radiation scattered from a plant stack emission allows one to make a remote real-time monitoring of the atmospheric pollutions. Devices for remote passive microwave radiometry of the atomic hydrogen in the emission plumes from nuclear plants are promising for monitoring industrial nuclear processes. A raster atmospheric-hydrooptical lidar was used for detecting the aerosol (hydrosol) stratification by the method of multiangular sounding. It also can be used for detecting weak emissions. The radiophysics-based techniques for single-wave measurements of the regular or random optical refraction as well as a universal interactive software designed for calculating the atmospheric corrections are promising for estimations of the efficiency of laser opto-electronic systems operating under different optical-climatic conditions in the ABL.

A TECHNIQUE OF PASSIVE CORRELATION SPECTROSCOPY OF THE GAS AND AEROSOL ANOMALIES AND THE EMISSION PLUMES FROM INDUSTRIAL PLANTS

Passive correlation spectroscopy, based on the use of "gaseousB filters enabling high-resolution selection of the molecular absorption bands of a gas studied among the overlapping lines and bands of foreign gases,[1–3,23] is used in a measurement method developed by the authors. This method takes into account the following factors: meteorological visual range in the atmosphere, the content of aerosol particles in the emission plume, azimuth of plume sighting relative to the direction to a local source of radiation or distributed illumination of daytime sky as well as the velocity of the emission jet outflow from stack determined from optical measurements.

The statistical approach to determining and estimating the parameters of gas anomalies, enables one to define the mean values and variance of the optical thickness of the anomaly, the correlation radius, the spatial frequency range and the mean area of the regions with the same optical thickness.

Remote detector of industrial emissions "DIVB has been created in two modifications, one in the near UV (0.3–0.4 μm) and the other one in IR (3–4.5 μm) spectral ranges. The maximum sounding distance is up to 5000 m, the measurement range of the volume concentration is $10^{-4}/D$–$10^{-5}/D$, where D, in m, is the emission plume diameter. The following gases can be detected: NO_2, NO, SO_2, I_2, H_2S, CH_4. The measurement process control, data processing and gas-anomaly visualization are realized using an IBM PC in a real time. The UV detector "DIV-1B was certified at Mendeleev All-Russian Scientific Research Institute (certificate No. 2421/902-92/2999). The experimental data on propagation of aerosol-gas emissions for different types of anomalies in the ABL have been obtained.

Methods of the correlation spectroscopy with the "gasB correlation filter are based on the use of a cell containing a gas (or mixture) to be detected in the atmosphere. The transmission coefficient $\langle T_c \rangle$ within the transmission band of the filter *3* is written as[4]:

$$\langle T_c \rangle = \int_{\Delta} u(\omega)\, T_c(\omega)\, d\omega \left[\int_{\Delta} u(\omega)\, d\omega \right]^{-1},$$

where $u(\omega)$ is the spectral intensity of the illuminating radiation, $T_c(\omega)$ is the function of spectral transparency

0235-6880/97/10 744-10 $02.00

of an absorbing gas. One carries out the calibration of the transmission of the correlation channel $\langle T_c \rangle$ and the reference one $\langle T_r \rangle$ (in the anomaly-free atmosphere) to provide the validity of the equation: $T_r = \langle T_c \rangle$.

If the background spectral transmission is $T_g(\omega)$, the correlation channel records the total transmission $\langle T_c, T_g \rangle$, whereas the reference channel records the signal value $\langle T_g \rangle T_r$. Thus, the difference of these signals normalized to their sum is written as follows:

$$A_g = \frac{\langle T_c \cdot T_g \rangle - \langle T_c \rangle \langle T_g \rangle}{\langle T_c \cdot T_g \rangle + \langle T_c \rangle \langle T_g \rangle} . \quad (1)$$

As a rule, $\langle T_g \rangle / \langle T_c \rangle \gg 1$ and $\langle T_g \rangle \to 1$, that results in $A_g \approx 1 - \langle T_g \rangle$.

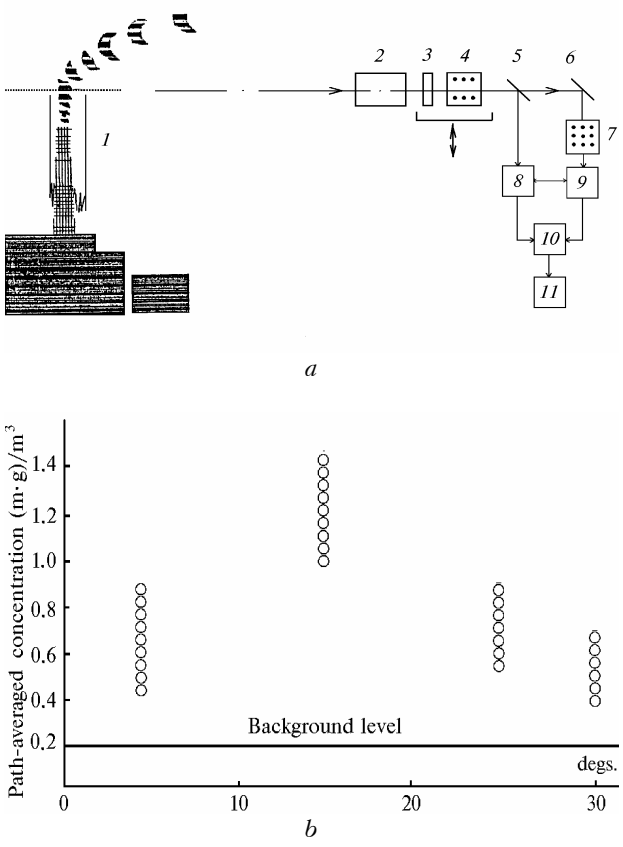

FIG. 1. Block-diagram and an example of remote azimuth measurements of NO_2 *in the emission plume of the industrial carbon. Densitogram of the absorption optical thickness of* NO_2 *in* 0.3–0.4 μm *spectral range (1), quartz objective (2), interference filter (3), set of the calibration cells (4), semitransparent plates (5 and 6), correlation gas filter (7), photo-receivers with amplifiers (8 and 9), electronic units for processing and visualization of the information (10 and 11) (a) and example of remote measurements (distance* 1 km*) of the azimuth dependence of* NO_2 *path-averaged concentration in an emission plume (perpendicular direction to the wind velocity vector) (b).*

In real atmospheric conditions there appear some problems related to the separation of the direct radiation and the lateral light scattering due to aerosols as well as to the meteorological conditions account.[2] Figure 1 shows the block-diagram (*a*) and an example (*b*) of the remote measurements of the NO_2 content in the emission plume from an industrial plant.

Note that the methods developed based on the analysis of correlation between the emission constituents concentrations and model devices for the passive correlation radiometers[1,2,4] operating in visible and IR enable one to monitor and identify some industrial plants dangerous for the environment, e.g. nuclear plants and thermal power stations.

PASSIVE RADIOMETRY OF ATOMIC HYDROGEN OVER A NUCLEAR PLANT

Institute of Atmospheric Optics in cooperation with Tomsk State University and Siberian Physical-Technical Institute have developed and tested a model setup designed for the environmental monitoring of nuclear plants emissions. The operation principle of this device is based on receiving radiation from the atomic hydrogen (at the wavelength 21.1 cm) which is the product of interaction between the radioactive elements and atmospheric gases. The basic principle of this technique is described in Ref. 5 (see Refs. 6 and 7 for a more detail).

A characteristic feature of the emissions from the nuclear fuel processing plants is the emission of radioactive isotopes. Analysis of the emissions from nuclear plants operating in a closed cycle[6,8] has shown that the most significant from the emitted elements was the isotope ^{85}Kr. According to Ref. 6, the annual emission of the ^{85}Kr is $1.6 \cdot 10^7$ Curie for radiochemical plants with the productivity of 1500 tons per year. The radioactivity of every m^3 of the emission is $6 \cdot 10^8$ Bq.

Enormous volumes of air (up to 10 km^3) surrounding the body of the emission plume are exposed to the radioactive irradiation. According to the results from Ref. 6, the atomic hydrogen concentration in the emission plume can reach 10^{-16}. The power of the noise radiation at the given frequency with the account of the atmospheric extinction is 10^{-19} W. The use of high sensitive detectors enables one to reliably detect the atomic hydrogen which is an indicator of radionuclides in the emissions from radiochemical plants.

An example of the spectrum recorded when observing along the direction to a nuclear processing plant (i.e. corresponded to a maximum of radiation)[7] is shown in Fig. 2.

The results of experiments have confirmed the possibility of using the technique for detecting the atomic hydrogen radiation in the emission plumes of nuclear plants. It conforms to the model described in Ref. 6. Thus, the above considered technique is much promising for monitoring nuclear plant processes, and its high sensitivity allows the detection of nuclear objects at long distances.

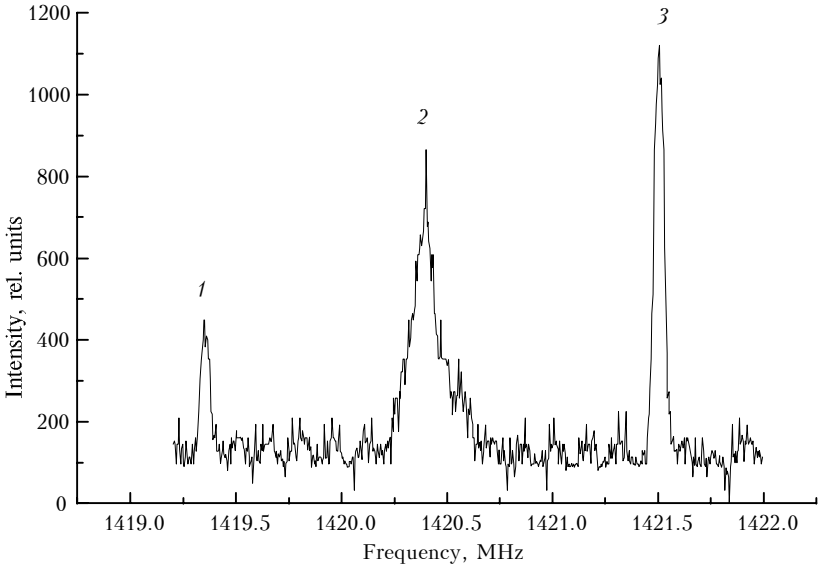

FIG. 2. Oscillogram of the received signal: frequency markers at 1419.348 *and* 1421.505 MHz (*1, 3*) *and signal from the emission plume (2).*

COHERENT OPTICAL METHOD FOR MEASUREMENTS OF THE AEROSOL PARTICLES MICROSTRUCTURE IN TURBULENT ATMOSPHERE

A coherent optical method for measuring the aerosol particle size distribution function[9] based on the statistical spatial filtration of the fluctuations in the optical image of particles in a receiving system has been developed.

The coherent or incoherent illumination of particles can be done from sources on both sides of the particle flux studied. Thus, one can use two schemes of illumination: a reflection method and a "radiographic" method. It is also possible to use the emission of particles initiated, for example, by intense laser radiation. The particles are assumed to be in a gas (e.g., in the atmosphere) or in liquid and diffusely reflects optical waves (for the coherent illumination). The particle size must exceed the maximum wavelength of the illumination radiation.

The image recorded with a receiver is split into a series of channels. In each channel a phase modulation of the radiation is performed at difference frequencies, using diffraction gratings with different distances between grooves.[10] It is also admissible to use only one channel equipped with the variable-period diffraction grating. One measures a time correlation function of the optical flux $P(\tau, \xi)$ (reflected or passed through the flux of particles depending on the illumination scheme) collected with the receiving telescope:

$$B_P(\tau, \xi_1, \xi_2) = \langle P(t_1, \xi_1)\, P(t_2, \xi_2)\rangle -$$

$$- \langle P(t_1, \xi_1)\rangle \langle P(t_2, \xi_2)\rangle,$$

where $\tau = t_2 - t_1$ is the time shift between the observation moments in time t_1 and t_2; ξ_1, ξ_2 are the spatial frequencies of the diffraction gratings corresponding to periods $d_1 = 2\pi/\xi_1$, $d_2 = 2\pi/\xi_2$. By using the spatial correlation coefficient of the optical flux $b_P(0, \xi, \xi) = B_P(0, \xi, \xi)/B_P(0, 0, 0)$, the following expressions allowing the restoration of the particle size distribution function $P_r(a)$ have been derived[9]:

$$S_4(X)/S_4(0) = \varphi(z\sqrt{2X}/F_0), \quad X = 2\left[\frac{\pi F_0}{z\, d}\right]^2,$$

$$d = \frac{2\pi}{\xi}, \quad S_4(X) = \int_0^\infty P_r(a)\, a^4 \exp(-X a^2)\, da; \qquad (2)$$

$$\varphi(\xi) = \begin{cases} 2(4b_P(0, \xi, \xi) - 1)\exp(2(a_0\xi/2)^2), & \xi > 2/a_P, \\ 2b_P(0, \xi, \xi) - 1, & \xi < 2/a_P, \end{cases}$$

where a is the radius of particles; z is the optical path length; F_0 is the distance from the plane of the receiving telescope lens to the square-law photo-detector with the radius a_p; a_0 is the radius of a point source image at the plane F_0.

The Eq. (2) shows that the size distribution function can be restored using the inverse Laplace transformation of the correlation coefficient of the received photoelectric current (note that the $S_4(0)$ constant can be found from the normalization conditions).

For aerosols of the industrial origin (e.g. at a stack mouth, the size distribution function is known to be described by the logarithmic normal distribution.[11] In this case, one needs only to find the unknown parameters of such distribution (i.e., the variance and average value) using a set of values of the time correlation function of a spatially-modulated optical flux, recorded with a photo-detector. Numerical

methods confirmed the stability of the algorithm for the retrieval of statistical characteristics of the aerosol particles size. This method was found to allow remote measurements of the velocity of the particle motion in a gas flow,[9] i.e. it allows the determination of the wind velocity in the atmosphere.

COHERENT LASER REFRACTOMETRY OF THE ATMOSPHERIC ANOMALIES

The atmospheric geochemical, the microclimate, and manmade anomalies in the ABL are known to result in regular variations of the refractive index. That is why, it is possible to inspect them using the measurements of the refractive deflections of the path of the optical waves propagating through the atmosphere.

The random and regular optical refraction can be an indicator of the turbulent fluxes in the ABL caused, for example, by a break of oil-pipe-lines and hot-water systems, fires, and emissions from the industrial plants.

Accurate angular measurements of the turbulent broadening of the angular spectrum of the wave require the account for a correction for regular refraction. The traditional theory of regular optical refraction uses the geometrical optics approximation[12,13] which results in some limitations concerning the propagation path length, and requires information on the initial dispersion properties of a refracting medium. The latter requires the use of optical radiation at several wavelengths. On the other hand, in terms of the radiophysics approach (see experimental and theoretical researches[14–16]), it was shown that the diffraction properties of a receiving radiation could result in significant effects on measurements of the refraction angle by a phase-sensitive receiving system.

The authors have developed a radiophysics-based technique for calculations of the refraction angles on the base of single-wave measurements. This method uses the coherent laser effects in the plane and spherical waves. The precision adaptive laser meter of the regular and random optical refraction has been developed.[10,17–19]

The deflection of a beam path can be described by the following angles: angle of the total geodetic refraction $\boldsymbol{\sigma}$ determined by the angle of the crossing of tangents to the beam path, restored at the points corresponding to the radiation source and receiver; refraction angles $\mathbf{r}_{12}$ (at the radiation source point) and $\mathbf{r}_{21}$ (at the receiver's point) which are defined by the angles between a straight line, connecting the emission and receiving points, and the corresponding tangents to a curvilinear path. In this case $\sigma = = \mathbf{r}_{12} + \mathbf{r}_{21}$. To derive the value of the angle σ, one needs to carry out simultaneous measurements of zenith angles Θ_{12} and Θ_{21} that lead to the following expression $\sigma = \pi - (\Theta_{12} + \Theta_{21})$.

The formulas for regular refraction angles $\mathbf{r}_{12}$ and $\mathbf{r}_{21}$:

$$\mathbf{r}_{12} = \frac{z}{2} \int_0^1 (1 - \xi)\, [\nabla_{\mathbf{p}}\, \nu(\xi, \mathbf{p})]_{\mathbf{p}=0}\, d\xi;$$

$$\mathbf{r}_{21} = \frac{z}{2} \int_0^1 \xi\, [\nabla_{\mathbf{p}}\, \nu(\xi, \mathbf{p})]_{\mathbf{p}=0}\, d\xi,$$

where z is the optical path length; $\mathbf{p} = (x, y)$ is the vector of the transverse coordinates; $[\nabla_{\mathbf{p}}\, \nu(\xi, \mathbf{p})]_{\mathbf{p}=0}$ is the transverse gradient of the dielectric constant, can be derived using the expression[18]:

$$\alpha_t = \mathbf{r}_{21} - \frac{\rho}{z} + R(z) \left(\mathbf{r}_{12} + \frac{\rho}{z} + \alpha \right); \qquad (3)$$

$$R(z) = \frac{1 - \frac{z}{F} + \frac{a_t^2}{a^2} \left[1 + \frac{z}{l} - \frac{z}{F_t} \right]}{\left[1 - \frac{z}{F} \right]^2 + \frac{z^2}{k^2 a^4} \left[1 + \frac{a^2}{\rho_k^2} \right] + \frac{a_t^2}{a^2}},$$

where α_t is the refraction angle at the receiver; α is the inclination angle between the axis of the laser radiation source and the receiver axis; F, $k = 2\pi/\lambda$, a, ρ_k, ρ are parameters of the laser radiation source, namely: the phase front curvature radius at the emitting aperture, wave number, radius of the emitting aperture, the coherence radius, the transverse vector of the distance from the receiver's optical axis to the center of the laser radiation source; a_t, l, F_t are the parameters of the receiver, namely: the input aperture radius, the distance from the center of the input lens to the image processing plane, and the focal length.

Equation (3) relates refraction angle α_t, at the receiver, measured in the atmosphere making the turbulence fluctuations averaging, the angle α known due to the receiver and source calibration and three unknown vectors: ρ, $\mathbf{r}_{12}$, and $\mathbf{r}_{21}$. The value of the angle $\mathbf{r}_{12}$ can be expressed in terms of $\mathbf{r}_{21}$ if the whole optical path is divided into a series of segments with the homogeneous underlying surface possessing constant gradient of the dielectric constant (in particular, the length of the above mentioned segments can reach ten kilometers for example over sea).

To derive unknown values ρ and $\mathbf{r}_{21}$ from Eq. (3), one needs to set up a set of two-vector equations different by the value of R parameter. In this case, one obtains essentially different values of R, if a plane ($R = 0$) and a spherical ($R = 1$) wave are generated in a succession with the same laser radiation source.

The following is a brief description of the adaptive laser device "LIRAB"[17–19] designed for measurements of the regular and random optical refraction.

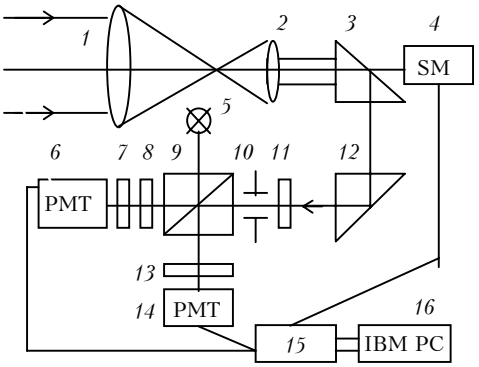

FIG. 3. Block-diagram of the adaptive laser refractometer "LIRAB: objective (1), eye piece (2), prism of the servodrive (3), stepper motor of the servodrive (4), adjustment lamp (5), PMT (6 and 14); light scatterer (7 and 13), optical analyzer of the image (8), beam splitter (9), field stop diaphragm (10), light filter (11), prism (12), the meter controller (15), and computer (16).

Block-diagram of the setup is shown in Fig. 3. The device consists of the optical path of a non-aberration telescope, the photometric unit, the precision rotating mechanism, the control processing block equipped with an IBM compatible computer, and a remote block of a single-mode laser transmitter with a theodolite 2T2.

The operation of this device is based on the determination of instantaneous refraction angle by measuring the energy center of mass of a remote source image (using a mathematical expression for the energy center of mass). The rate of measurements was up to 1000 Hz, the field of view angle was 100 seconds of arc. To extend the vertical field of view up to 2.0 degrees, the IBM computer controlled servodrive equipped with a stepper motor was used. The servodrive makes (every 100 seconds) corrections of the source image position at the optical axis of the receiving system: namely, the correction by the angle equal to the average deviation of an image center of mass during a 100-second time interval.

The measured values of the average refraction angles ranges from 0.2 to 200 seconds of arc, with the error of measurements of 0.2 second of arc. The range of the relative variance of the angular diffraction is 0.1–10 second of arc. The atmospheric path length is 0.5–30 km. The laser radiation source wavelength is 0.63 μm. The use of the laser sources with other wavelengths is admissible.

RASTER ATMOSPHERIC AND HYDROOPTICAL LIDAR

The conception of using a multipurpose high-transmission lidar equipped with a raster-type diffraction spectrometer for detection of weak night sky emissions and emissions from the ocean upper layer was discussed in Refs. 4, 20–23. The lidar technique of multiangular sounding without any *a priori* information on the lidar ratio was used for diagnostics of plane scattering layers in the ocean upper layer and the atmosphere above it.

The block-diagram of the lidar is shown in Fig. 4. Lidar was mounted in a mobile van. An industrial LTI-type pulsed laser with frequency doubling of the output radiation is used as a source (blocks *3*, *4*) of sounding radiation.

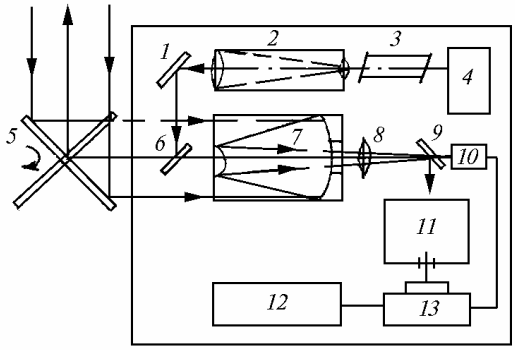

FIG. 4. Block-diagram of the raster atmospheric optics lidar: optical components (1, 2, 5, 6, 7, 8, and 9), the laser radiation sources (3 and 4), PMTs (10 and 13), raster monochromator (11), and personal computer (12).

The radiation wavelength is 532 nm, the pulse duration is 15 ns, the pulse repetition frequency is up to 12.5 Hz, the average power of generation is up to 1 W. The laser radiation is directed into the atmosphere or toward the sea surface (maximum distance is 10 km) through a collimator *2* and a system of steering mirrors *1*, *5*, *6*. The radiation, reemitted by the media, is focused with a Cassegrainian receiving telescope *7* (diameter of the primary mirror is 500 mm) on the input slit of a raster double monochromator *11* or on the block of PMTs *10*. The PMT *13* records the spectrum of the radiation received from the monochromator.

The double raster monochromator is used to increase (by 10 times) the lidar transmission.[4] The main principle of the raster filtration is to provide the passage of a quasi-monochromatic (i.e. in a narrow spectral interval) radiation through the monochromator along some different (N) optical paths with close optical thicknesses and to detect it with a single detector. In order to reach this effect, we use multislit arrays in a standard monochromator with the dispersion summation instead of three single-slit blocks. The design of the above mentioned rasters provides the same instrumental function (as it was for a single-slit raster) and the increase of the transmission which is proportional to the number N of slits in the rasters. In this case a multislit raster has 10 slits.

The lidar signals can be detected using the unit *10* both in the analog and in a photon counting modes with the frequency up to 50 MHz.

Multiangular method of laser sounding[20] of the optical thickness $\tau(h_k)$ of the plane aerosol (hydrosol)

layers situated at an altitude (depth) h_k is based on the expression that follows from the lidar equation:

$$d[\ln S(h_k, \psi)]/d\psi = -2\tau(h_k),$$

where $\psi = \sec(\gamma)$, γ is the zenith angle at which the aerosol layer is sounded; $S(h_k, \psi) = u\, h_k^2\, \psi^2/C_0$, where u is the amplitude of the lidar return from the layer; $\Delta h_k = h_{k+1} - h_k$; C_0 is the lidar constant.

The problem of differentiation of a random function (lidar signal) is known to be an ill-posed problem and, thus, it requires the use of regularization algorithms. We use the following algorithm:

$$\tau_a(h_k) = -0.5\, d[\ln S^{(a)}(h_k, \psi)]/d\psi;$$

$$S^{(a)}(h_k, \psi) = S(h_k, \psi_a) + \int_{\psi_a}^{\psi} \mu(h_k, \psi')\, d\psi',$$

where $\mu(h_k, \psi) = d[\ln S^{(a)}(h_k, \psi)]/d\psi$ is the regularized value of the lidar return logarithmic derivative with respect to y at a fixed fit parameter "aB

In this case, the problem of filtration of regular components of a signal with random noises to be differentiated is reduced to the solution of the Fredholm integral equation of the first kind using Tikhonov[24] method of smoothing functional.

Some examples of the lidar returns from the atmosphere and the upper layers of sea water multiplied by squared distance, h^2, are shown in Fig. 5. The plots correspond to different angles between the beam axis and the normal to the water surface (for experiments in the atmosphere), and angles between the normal and the incidence direction minus $\pi/2$ for experiments in the sea water.

The peaks of the lidar returns observed in Fig. 5 (right peaks at $(\gamma - \pi/2) = 35$ and 45 angular degrees) are attributed to the reflection from the sea bottom, at the depth $h = 25$ m.

By processing the signals of the fluctuating component due to reflection from the sea surface allows the determination of the sea wave spectra in the frequency range corresponding to the energy carrier and microcapillary waves.

Results of the treatment of lidar returns using the above mentioned method are presented in Fig. 6. The maximum of the scattering coefficient of the laser radiation at the altitude $h = 400$ m is caused by an aerosol layer.

The use of the raster monochromator also provides, in the passive mode, for recording the emission spectra of night atmosphere (Fig. 7). In particular, reliable identification of the emission spectra of the atomic H and Na from altitudes 80 to 100 km.

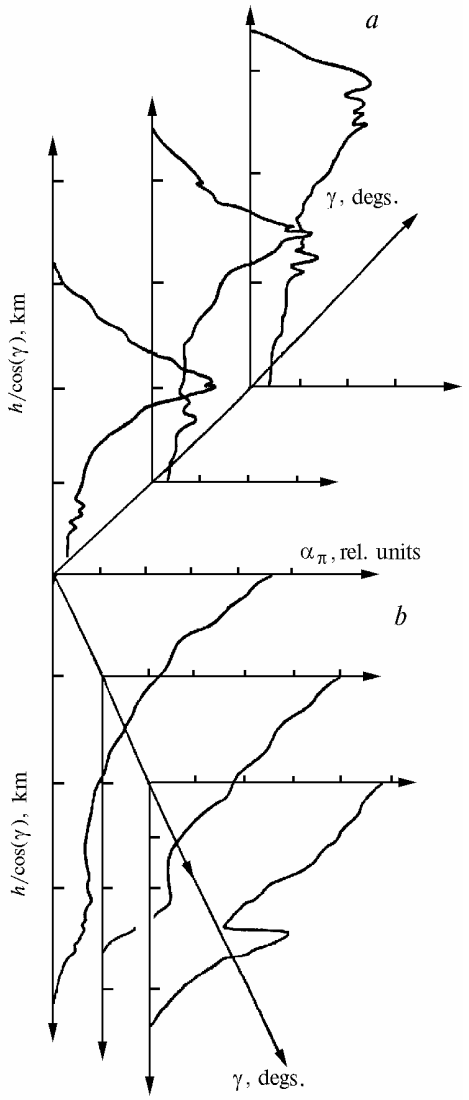

FIG. 5. Normalized histograms of the lidar echo-signals received at multiangular sounding of the atmosphere (a) and sea water (b).

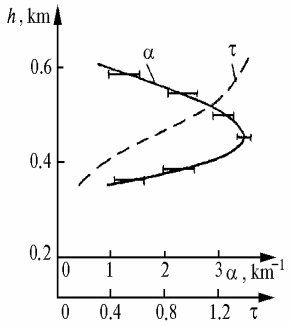

FIG. 6. Reconstructed profiles of the extinction coefficient (α) and optical thickness (τ) of the aerosol layer.

Figure 8 demonstrates the identification of the fluorescence spectra and concentration of sea salt using Raman scattering line of water as the reference spectral line.[25]

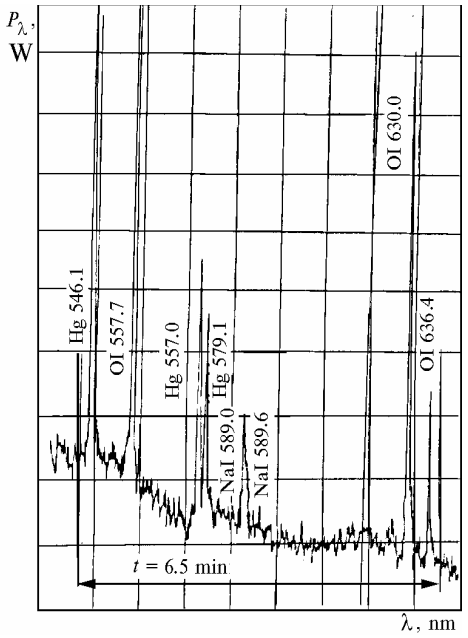

FIG. 7. An example of the emission spectrum of the night atmosphere recorded with the raster monochromator (the fall season, latitude 54 degrees).

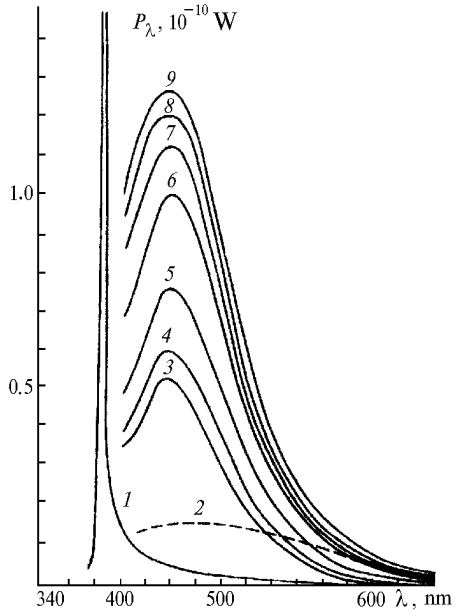

FIG. 8. The lidar fluorescence spectra of sea water (3–9) with relative concentration of the sea salt 1, 2, 5, 10, 15, 20, 25%*; the reference Raman signal from water (1) and* 20% *solution of pure* NaCl *(2).*

The developed lidar was used for *in situ* atmospheric-hydrooptical measurements, carried out in cooperation with the Marine Hydrophysical Institute of the Ukrainian Academy of Sciences, at a Black Sea coastal site (Katsiveli settlement).[20]

It should be noted that the possibilities of the lidar allow one to use it for the ground support measurements in satellite sounding dealing with the geographical calibration of the NOAA, Meteor-type satellites photometry measurements as well as in the lidar experiments from space-based platforms.

STATISTICAL APPROACH TO DETECTION AND ESTIMATION OF THE ATMOSPHERIC ANOMALIES OBSERVED AGAINST THE BACKGROUND FROM THE UNDERLYING SURFACE

In order to carry out a remote space-based sounding of the gas-aerosol atmospheric anomalies one makes the comparison of the spectral transparencies $T(\omega)$ within the absorption band $\Delta\omega_g$ of a gas (gas mixture) of interest and out of it $\Delta\omega_0$. That is why it is necessary to estimate the fields of the random value $A_g(\rho) = [T(\Delta\omega_g) - T(\Delta\omega_0)]/[T(\Delta\omega_0) + T(\Delta\omega_g)]$ against the background from the underlying surface, and of the value of $A_0 = A_0(\rho)$, $0 \le A_0(\rho) \le 1$, where $\rho = (x, y)$ is vector of the transverse (with respect to an optical path) coordinates of a surface point; $A_0(\rho)$ is called the coefficient of vertical diffuse reflection. The A_0 value is assumed to be independent of the wavenumber ω within the spectral range $|\Delta\omega_g - \Delta\omega_0|$. Thus, it is possible to carry out independent measurements of $A_g(\rho)$ and $A_0(\rho)$ using the same statistical methods for spatial filtration of images. The value $A_g(\rho)$ is called the effective spectral albedo of the gas anomaly. The following is a summary of the method for estimation of the statistical characteristics of the underlying surface albedo $A_0(\rho)$ developed by the authors.[26] This technique is good for description of the effective spectral albedo $A_g(\rho)$ for the turbulence caused anomalies.

Measurements of the spatial-frequency spectrum of the effective albedo allow the analysis of the information on a frequency composition of the surface parts size with the same structure. In particular, a "valleyB in the spatial frequency spectrum ($\omega_1 = 2\pi/l_1$, $\omega_2 = 2\pi/l_2$ where l_1, l_2 are the size of the parts) demonstrates that there are no surface parts with the size $l_2 < l < l_1$, possessing the same value of albedo, in the region under consideration. On the contrary the concentration of the spectrum in the (ω_1, ω_2) interval is indicative of the presence of such surface parts. The statistical characteristics of the surface parts with the same structure (albedo) (i.e., average cross section, the cross section variance) play an important role.

The function describing the random cross section S of all the surface parts with the same albedo, situated in the region of interest with the total cross section S_0, can be written as follows[26]:

$$S = \int_{S_0} d^2\rho\, \Theta\,(A_0(\rho) - I_A), \quad \Theta(x) = \begin{cases} 1; & x > 0, \\ 0; & x \le 0, \end{cases} \qquad (4)$$

where I_A is the threshold level (two surface parts are considered to be equal, if the surface albedo $A_0(\rho)$ exceeds this level). In the general case, one can

consider that the I_A value is equal to an average value of the background near the anomaly. The computations made by the authors resulted in the following expression for $<S>$ (average cross sections of all the surface parts with the same albedo)[26]:

$$<S> = \frac{S_0}{2}\left\{1 + \Phi\left[\frac{(<A_0> - I_A)^2}{2\sigma^2}\right] \operatorname{sgn}(<A_0> - I_A)\right\}; \quad (5)$$

$$\Phi(y) = 2\sqrt{y/\pi}\ {}_1F_1(1/2, 3/2, -y),$$

where σ^2 is the albedo variance, ${}_1F_1(a, b; -y)$ is the degenerate hypergeometric function. The peculiarities of the $\Theta(x)$ behavior require the information on the $A_0(\rho)$ values only if they are close to I_A. That is why, to derive the Eq. (4), one should use the approximation of the probability density $A_0(\rho)$ by the normal law. The latter can also be applied to modeling the random field of the gaseous anomalies in the turbulent atmosphere.

The Eq. (5) shows that the increase in I_A value ($I_A \gg <A_0>$) results in a decrease in $<S>$ down to zero, and vice versa, a decrease in I_A ($I_A \ll <A_0>$) leads to an increase in $<S>$ value and approaches the value

$$<S> = \frac{S_0}{2}\left[1 + \Phi\left(\frac{<A_0>^2}{2\sigma^2}\right)\right], \quad (6)$$

depending on the ratio $<A_0>/\sigma$.

The fine structure and peaks in the random field of the albedo correspond to small values of $<A_0>/\sigma$. This case is characterized by the average cross sections of the parts with the same albedo close to the average cross sections of the background parts with the value of albedo less then I_A. According to Eq. (6): $<S> \to S_0/2$.

As for the high values of the above mentioned ratio, the random function A_0 shows only small deviations from its average value. Thus, if $I_A << <A_0>$ one observes the random albedo exceeding the value I_A. That is why, according to Eq. (4), the whole surface of the region of interest is considered to have the same albedo, and Eq. (6) leads to $<S> \to S_0$.

Two methods for sounding the characteristics of the surface albedo fields have been developed in Ref. 26. Characteristics of the albedo fields are obtained using the theory of wave propagation in the randomly inhomogeneous media[27–31] and from analysis of fluctuations of an optical flux reflected from the Earth surface.

The first variant of the technique is called the two-beam since it uses two sources of optical radiation (coherent or incoherent), formed into two beams for the surface illumination, as well as two photodetectors for the reflected radiation analysis. The second variant of this technique, called the single-beam method, requires one optical radiation source (beam) and one receiver. Both the sources and receivers of radiation are mounted on a space-based platforms (e.g., planes, satellites, etc.). The use of the high spatial resolution spectrophotometers allows one to turn the second variant of the technique into the passive one for analyzing the statistics of the light flux from natural radiation scattered by the Earth surface.

The method[26] allows one to determine the following parameters: the average value and the variance of albedo, the time and spatial correlation functions, the radius of the albedo correlation, the spatial frequency spectrum as well as the average cross section of all the anomalous surface parts with the same value of albedo.

THE COMPUTER INTERACTIVE SOFTWARE FOR ESTIMATIONS OF THE EFFICIENCY OF THE OPTO-ELECTRONIC SYSTEMS OPERATING IN VARIOUS OPTICAL WEATHER CONDITIONS

There are many problems of the atmospheric optics, e.g., the laser sounding, image transmission, range finding, location, navigation, etc., requiring the real time scale information on the influence of optical effects in real atmosphere on the precision and energy characteristics of the opto-electronic systems operating under different microclimate conditions and anomalies.

The computer interactive software package (hereafter software), designed for forecasting and accounting for the influence of the linear optical effects in the atmosphere on characteristics of the optical radiation used in an opto-electronic device, has been developed in Ref. 32–33. The software is a package of the interactive computer programs. These programs are based on the engineering methods[34–36] developed at the Institute of Atmospheric Optics and involve the results of fundamental research in the atmospheric optics.

The software uses databases on the atmospheric optics parameters compiled for various geographical zones and comprising the information on the zone, seasonal, and diurnal variations of the altitude profiles for parameters of the atmospheric absorbing gases, aerosols, meteorological characteristics, characteristics of the turbulent air fluxes, and clouds. The database is based on the complex optical atmospheric model.[35] In addition, the software allows the effective account for corrections due to nonselective influence of the atmospheric aerosols and turbulence.

The software allows one to calculate the following characteristics:

1) correction for the range and regular refraction angle;

2) attenuation of optical radiation due to the molecular and aerosol absorption;

3) pulse characteristics and intensity of the backscattered radiation for different receiving apertures;

4) level of illumination due to natural noise sources (e.g., the scattered solar radiation, thermal

radiation of the underlying surface and the atmosphere);

5) energy and precision characteristics of opto-electronic systems operating under the atmospheric turbulence conditions.

The software is an open flexible system that is easy to modify to meet a wide range of the atmospheric optics problems, e.g., the forecast of the optical characteristics of both the ground-based setups and that operating from aerospace platforms.

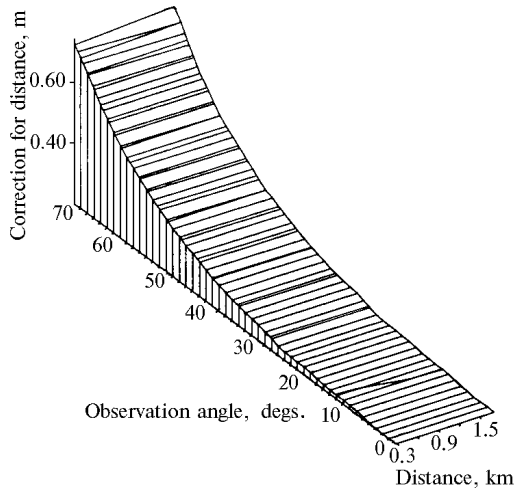

FIG. 9. Estimation of the correction for distance. Conditions of the experiment: observation angles from 0 *to* 70° *for* 0.1–2.5 km *distances to an object of observation; daytime; type of the optical weather: clear atmosphere; ground-based lidar; visibility range* 13 km.

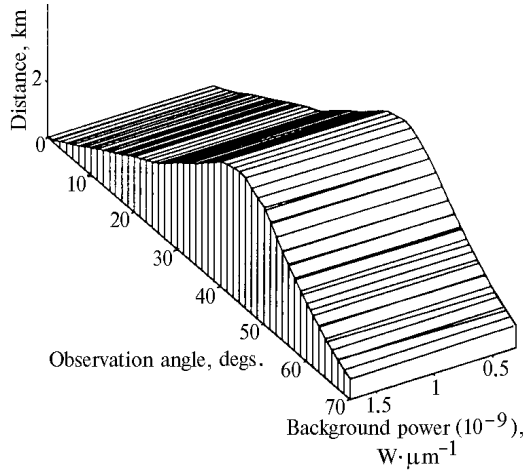

FIG. 10. Distribution of the clear sky spectral intensity at 10.6 μm. *The conditions of the experiment: the "grass-forestB type of the underlying surface; azimuth of the Sun* – 180°*; angular height of the Sun* – 45°*; the same weather conditions as in Fig. 9.*

Figures 9 and 10 illustrate applications of the software to computations of corrections for distance and the spectral intensity of the clear sky (for slant paths).

REFERENCES

1. Yu.D. Kopytin, V.I. Kokhanov, and S.A. Shishigin, Atmos. Oceanic Opt. **7**, No. 5, 350–352, (1994); Atmos. Oceanic Opt. **7**, No. 7, 531–532 (1994).
2. S.F. Balandin and Yu.D. Kopytin, in: *Proceedings of the First Inter-Republic Symposium on Atmospheric and Oceanic Optics,* (Institute of Atmospheric Optics, Tomsk, 1995), part 2, pp. 194–195, *Proceedings of the Regional Conference "Siberian AerosolsB* (Institute of Atmospheric Optics, Tomsk, 1995), p. 785.
3. V.P. Kabashnikov, A.A. Kurskov, and N.S. Makarevich, Zh. Prikl. Spektrosk. **14**, No. 6, 965–970 (1986).
4. V.V. Afanas'ev, I.A. Zinkin, Yu.D. Kopytin, and V.B. Shlishevskii, Opticheskii Zh., No. 2, 80–81 (1993).
5. E.T. Protasevich, Atmos. Oceanic Opt. **7**, No. 5, 353–354 (1994).
6. S.T. Penin and L.K. Chistyakova, Atmos. Oceanic Opt. **10**, No. 1, 45–49 (1997).
7. L.K. Chistyakova, V.Yu. Chistyakov, D.V. Losev, S.T. Penin, Yu.K. Tarabrin, V.P. Yakubov, and I.A. Yur'ev, Microwave and Optical Technology Letters, No. 11 (November), 1997.
8. N.S. Bataev and V.E. Demin, *Nuclear Industry and Environment* (Energoizdat, Moscow, 1984), 150 p.
9. V.V. Nosov, Atmos. Oceanic Opt. **9**, No. 1, 56–59 (1996)
10. V.V. Nosov, Opt. Atm. **1**, No. 1, 122–125 (1988).
11. V.E. Zuev and M.V. Kabanov, *Optics of the Atmospheric Aerosol* (Gidrometeoizdat, Leningrad, 1987), 254 pp.
12. M.A. Kolosov and A.V. Shebelnikov, *Refraction of the Electromagnetic Waves in the Earth, Venus and Mars Atmospheres* (Sov. Radio, Moscow, 1978) 220 pp.
13. A.V. Alekseev, M.V. Kabanov, and N.F. Kushtin, *Optical Refraction in the Terrestrial Atmosphere* (Nauka, Novosibirsk, 1982), 170 pp.
14. V.V. Vinogradov, A.G. Kosterin, A.S. Medovikov, and A.I. Saichev, Izv. Vyssh. Uchebn. Zaved. SSSR, Ser. Radiotekhnika **28**, No. 10, 1227–1232 (1985).
15. V.A. Banakh, A.E. Melamud, V.L. Mironov, V.V. Nosov, and B.N. Chen, Opt. Spektrosk. **62**, No. 5, 1136–1140 (1987).
16. V.A. Banakh, A.R. Larichev, V.M. Sazanovich, R.Sh. Tsvyk, and B.N. Chen, Atmos. Oceanic Opt. **3**, No. 3, 242–246 (1990).
17. Yu.D. Kopytin, V.V. Nosov, and E.V. Nosov, Izv. Vyssh. Uchebn. Zaved., Ser. Fizika, Dep., Registration No. 3158–B96, 1996, 25 pp.
18. Yu.D. Kopytin, V.V. Nosov, and E.V. Nosov, Izv. Vyssh. Uchebn. Zaved., Ser. Fizika, Dep., Registration No. 3159–B96, 1996, 36 pp.
19. Yu.D. Kopytin, V.V. Nosov, and A.I. Petrov, Izv. Vyssh. Uchebn. Zaved., Ser. Fizika, Dep., Registration No. 3432–B96, 1996, 9 pp.
20. Yu.D. Kopytin, S.F. Balandin, I.A. Zinkin, B.P. Ivanenko, K.D. Schelevoi, et al., in: *Proceedings of*

the IV All-Union Symposium on Propagation of Laser Radiation through the Atmosphere (Institute of Atmospheric Optics, Tomsk, 1989), Part 2, pp. 26–28.
21. N.F. Chaika and V.B. Shlishevskii, in: *Remote Studies of the Environment by Optical and Radiophysics Methods* (State University, Leningrad, 1983), pp. 95–105.
22. I.A. Zinkin and Yu.D. Kopytin, Inventor's Certificate No. 29/89, Bull. August 20, 1991.
23. Yu.D. Dunovskii, V.N. Ikkonen, and Yu.D. Kopytin, Inventor's Certificate No. 1689809, Bull. July 08, 1991; Inventor's Certificate No.1693300, Bull. Nov.r 10, 1991.
24. B.P. Ivanenko and I.E. Naats, Izv. Akad. Nauk SSSR, Fiz. Atmos. Okeana **19**, No. 1, 1210–1215 (1983).
25. M.A. Buldakov, Yu.D. Kopytin, S.V. Lazarev, and I.I. Matrosov, *Sounding of the Physico-Chemical Atmospheric Parameters Using High-Power Lasers* (Institute of Atmospheric Optics, Tomsk, 1989) pp. 211–219.
26. V.V. Nosov, The International Aerospace Sensing Conference. USA. Orlando. April, 1994. Proc. SPIE, 28–31 (1994).
27. K.Ya. Kondrat'ev, ed., *Radiation Characteristics of the Atmosphere and the Earth Surface* (Gidrometeoizdat, Moscow, 1969), 564 pp.
28. S.M. Rytov, Yu.A. Kravtsov, and V.I. Tatarskii, *Introduction into the Statistical Optics. Part II. Random Fields* (Nauka, Moscow, 1978), 464 pp.
29. V.I. Tatarskii, *Propagation of Waves through the Turbulent Atmosphere* (Nauka, Moscow, 1967), 548 pp.
30. A.S. Gurvich, A.I. Kon, V.L. Mironov, et al., *Laser Radiation in the Turbulent Atmosphere* (Nauka, Moscow, 1978), 277 pp.
31. N.K. Vinnichenko, N.S. Pirus, S.M. Shmetter, et al., *Turbulence in the Free Atmosphere* (Gidrometeoizdat, Leningrad, 1976), 336 pp.
32. E.B. Belyaev, G.B. Zhidkovskii, A.I. Isakova, Yu.D. Kopytin, and V.V. Nosov, Atmos. Oceanic Opt. **5**, No. 7, 488–491 (1992).
33. E.B. Belyaev, A.I. Isakova, Yu.D. Kopytin, and V.V. Nosov, Atmos. Oceanic Opt. **6**, No. 10, 754–758 (1993).
34. M.S. Belen'kii, G.O. Zadde, V.S. Komarov, et al., *Optical Model of the Atmosphere* (Tomsk Affiliate of the Siberian Branch of the Academy of Sciences of the USSR, Tomsk, 1987), 225 pp.
35. V.P. Aksenov, A.V. Alekseev, V.A. Banakh, et al., *Atmospheric Effects on the Laser Radiation Propagation* (Tomsk Affiliate of the Siberian Branch of the Academy of Sciences of the USSR, Tomsk, 1987), 247 pp.
36. E.B. Belyaev, V.V. Vorob'ev, A.A. Zemlyanov, et al., *Non-linear optical phenomena in the atmosphere*, (Tomsk Affiliate of the Siberian Branch of the Academy of Sciences of the USSR, Tomsk, 1987), 224 pp.
37. Yu.D. Kopytin, A.I. Isakova, E.B. Belyaev, and V.V. Nosov, in: *Proceedings of the International Symposium on Optical Science, Engineering, and Instrumentation,* San Diego, California, USA, 27 July-1 August 1997.